

Probabilistic Constellation Shaping for Enhancing Spectral Efficiency in NOMA VLC Systems

Amanat Kafizov, *Student Member, IEEE*, Ahmed Elzanaty, *Senior Member, IEEE*, Mohamed-Slim Alouini, *Fellow, IEEE*

Abstract—The limited modulation bandwidth of the light emitting diodes (LEDs) presents a challenge in the development of practical high-data-rate visible light communication (VLC) systems. In this paper, a novel adaptive coded probabilistic shaping (PS)-based nonorthogonal multiple access (NOMA) scheme is proposed to improve spectral efficiency (SE) of VLC systems in multiuser uplink communication scenarios. The proposed scheme adapts its rate to the optical signal-to-noise ratio (OSNR) by utilizing non-uniformly distributed discrete constellation symbols and low complexity channel encoder. Furthermore, an alternate optimization algorithm is proposed to determine the optimal channel coding rate, constellation spacing, and probability mass function (PMF) of each user. The extensive numerical results show that the proposed PS-based NOMA scheme closely approaches the capacity of NOMA with fine granularity. Presented results demonstrate the effectiveness of our scheme in improving the SE of VLC systems in multiuser scenarios. For instance, our scheme exhibits substantial SE gains over existing schemes, namely, the pairwise coded modulation (PCM), geometric shaping (GS), and uniform-distribution schemes. These findings highlight the potential of our approach to significantly enhance VLC systems.

Index Terms—NOMA; probabilistic shaping; VLC; performance analysis; spectral efficiency

I. INTRODUCTION

The exponential growth in the number of Internet of Things (IoT) devices has led to a significant demand for high data rates in wireless traffic. However, traditional radio frequency (RF) communication systems face challenges in meeting this demand due to limited spectrum resources. As a promising high-speed alternative and complementary technique to RF, visible light communication (VLC), which utilizes light emitting diode (LED) devices for both illumination and data transmission, has attracted considerable research attention [1]. Nonetheless, the development of practical high-data-rate VLC systems is hindered by the narrow modulation bandwidth of LEDs [2]. As a result, numerous techniques, encompassing advanced multiple access schemes, multiple-input multiple-output (MIMO), reconfigurable intelligent surface (RIS), and frequency reuse methods, have been explored to enhance spectral efficiency (SE) of VLC systems. Nevertheless, a shared limitation in these methodologies is their reliance on a

uniform symbol distribution, resulting in a gap loss from the channel capacity [3]–[6].

Recently, constellation shaping techniques have emerged as a method to improve the SE of communication systems, mitigating the aforementioned gap loss. In general, to achieve the channel capacity with a given transmitted power constraint, the input to the channel should have a capacity-achieving distribution. However, the actual input distribution often deviates from the capacity-achieving one, resulting in a shaping gap between the achievable rate (AR) and the channel capacity [7]. Probabilistic shaping (PS) and geometric shaping (GS) are widely known techniques that aim to reduce this shaping gap by optimizing the probability and location of the constellation symbols, respectively. Compared to GS, PS offers greater flexibility for granularity and enables easy implementation of Gray mapping [8], [9]. Importantly, it's worth noting that constellation shaping doesn't conflict with existing techniques used to enhance the SE of VLC systems. Instead, it can be combined with these techniques to further enhance the SE of VLC systems.

Authors in [10] propose a practical PS technique based on reverse concatenation architecture, where distribution matcher is applied before a systematic channel encoder at the transmitter. In [10], uniform information bits are practicably transformed into symbols with desired distribution by constant composition distribution matcher (CCDM). The symbols with low energy are transmitted more frequently than the high energy symbols. Thus, the available bandwidth is efficiently utilized. The advantages of this architecture have led to its widespread adoption in optical communications. For example, the work in [11] proposes an adaptive modulation scheme based on PS for free space optics (FSO) channels, providing a solution for FSO backhauling in terrestrial and satellite communication systems to achieve higher SE. In [12], authors propose adaptive spatial modulation (SM) scheme with PS, where either the spatial or constellation symbols are probabilistically shaped, to improve the transmission rate (TR) of VLC systems. However, existing works primarily focus on point-to-point (P2P) communication scenarios.

In real-world VLC systems, where a single LED transmitter is typically expected to accommodate multiple users, addressing the challenge of serving multiple users has led researchers to propose advanced schemes for multiple access channel (MAC). While orthogonal multiple access (OMA) techniques have been designed for VLC systems, researchers are exploring nonorthogonal multiple access (NOMA) techniques to efficiently increase the SE of VLC systems [13]. Among

A. Kafizov and M.-S. Alouini are with Computer, Electrical, and Mathematical Science and Engineering (CEMSE) Division, King Abdullah University of Science and Technology (KAUST), Thuwal, Saudi Arabia (email: {amanat.kafizov, slim.alouini}@kaust.edu.sa).

A. Elzanaty is with the Institute for Communication Systems (ICS), Home of the 5G and 6G Innovation Centres (5GIC and 6GIC), University of Surrey, Guildford GU2 7XH, United Kingdom (e-mail: a.elzanaty@surrey.ac.uk).

the various NOMA techniques, power domain NOMA stands out as a widely adopted approach, wherein multiple users are served over the available time and frequency resources using different power levels [14]. NOMA offers several benefits such as low transmission latency, improved SE and higher cell-edge throughput. The NOMA symbol is generated by superposing signals from multiple users, while successive interference cancellation (SIC) is employed at the receiver for signal detection [15].

In order to examine the interaction between NOMA and VLC, researchers in [15] presented a mathematical framework to assess the average performance of NOMA VLC systems. The analytical findings demonstrated that NOMA VLC surpasses OMA VLC in terms of the coverage probability, particularly in high optical signal-to-noise ratio (OSNR) conditions. The study also revealed that by increasing the discrepancy in channel gains between paired users and selecting appropriate LEDs, the benefits of NOMA can be further amplified. In [13], the authors aim to maximize the sum rate by optimizing the power allocation for each user in a power-line-fed VLC network. The efficient channel estimation method for minimizing the bit error rate (BER) in the optical MIMO NOMA-VLC is proposed in [16]. In [17] and [18], the NOMA-based hybrid VLC/RF systems are presented with design objectives as outage probability and the sum rate, respectively. However, these works consider uniform signaling, which leads to the shaping gap.

In contrast, authors in [19] examine the application of PS in NOMA VLC. However, this study encounters significant issues. Firstly, the adopted analysis methods, specifically the choice of AR, are unsuitable for the VLC domain. Secondly, the sum rate constraint of the capacity region of optical multiple access channel (OMAC) is disregarded. Thirdly, essential properties such as limited average and/or peak optical power and the non-negativity of optical intensity are violated. Consequently, there is a lack of extensive research in analyzing the performance of PS in NOMA VLC systems, which necessitates further exploration.

Table I: Comparison between proposed and typical works.

Work	Constellation Shaping	Frequency Band Type	Channel Type	Optimization Objective
Proposed	Yes	VLC	MAC	Transmission rate
[10]	Yes	RF	P2P	Transmission rate
[11]	Yes	FSO	P2P	Achievable rate
[12]	Yes	VLC	P2P	Transmission rate
[13]	No	VLC	MAC	Sum rate
[15]	No	VLC	MAC	Coverage probability
[16]	No	VLC	MAC	BER
[17]	No	Hybrid VLC/RF	MAC	Outage Probability
[18]	No	Hybrid VLC/RF	MAC	Sum rate
[19]	No	Unsuitable for VLC	MAC	Entropy

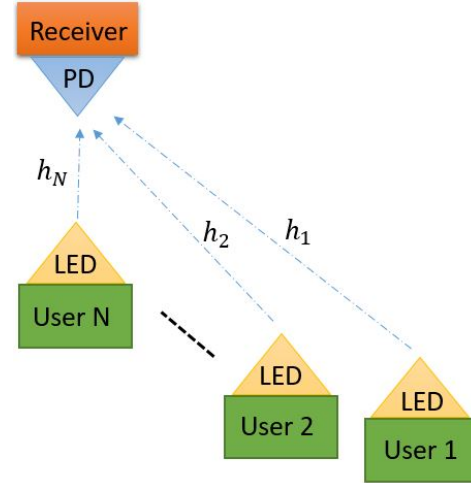


Figure 1: Uplink NOMA transmission scenario for N users.

In Table I, we provide a succinct overview of the key attributes of the discussed works and our proposed scheme for better clarity and comparison. Table I summarizes key characteristics of these works, focusing on aspects such as constellation shaping, frequency band type, channel type and optimization objective. As highlighted in the table, traditional NOMA VLC systems typically adopt uniform input signals, where constellation shaping is an area yet to be fully explored to mitigate shaping loss for each user. Unlike existing schemes, our proposed adaptive coded PS-based NOMA scheme effectively adapts its rate to the OSNR by utilizing non-uniformly distributed discrete constellation symbols. This adaptive strategy, coupled with a low-complexity channel encoder and an alternate optimization algorithm, leads to substantial gains in SE for VLC systems in multiuser uplink scenarios. The extensive numerical results showcase the scheme's ability to closely approach the capacity of NOMA, outperforming existing schemes such as pairwise coded modulation (PCM), GS, and uniform-distribution schemes.

A. Main Contributions

In this paper, we propose a novel adaptive coded PS-based NOMA scheme designed to further improve the SE of VLC systems in multiuser uplink scenarios. At the encoder of the proposed scheme, the uniform information bits are practicably transformed into unipolar M -PAM symbols with desired distribution by CCDM [20], laying the foundation for adaptability in our proposed scheme. An efficient forward error correction (FEC) encoder is then applied to generate uniformly distributed parity bits. The uniformly distributed unipolar M -pulse amplitude modulation (PAM) symbols are produced from the parity bits using the binary demapper. After that, multiplexer appends probabilistically shaped and uniformly distributed symbols to form a codeword. At the decoder, distribution dematching is performed after FEC decoding. There is an optimization problem for each user that needs to be solved to determine the capacity-achieving distribution. By probabilistically shaping the distribution of the unipolar M -PAM symbols and optimizing their constellation spacing, the

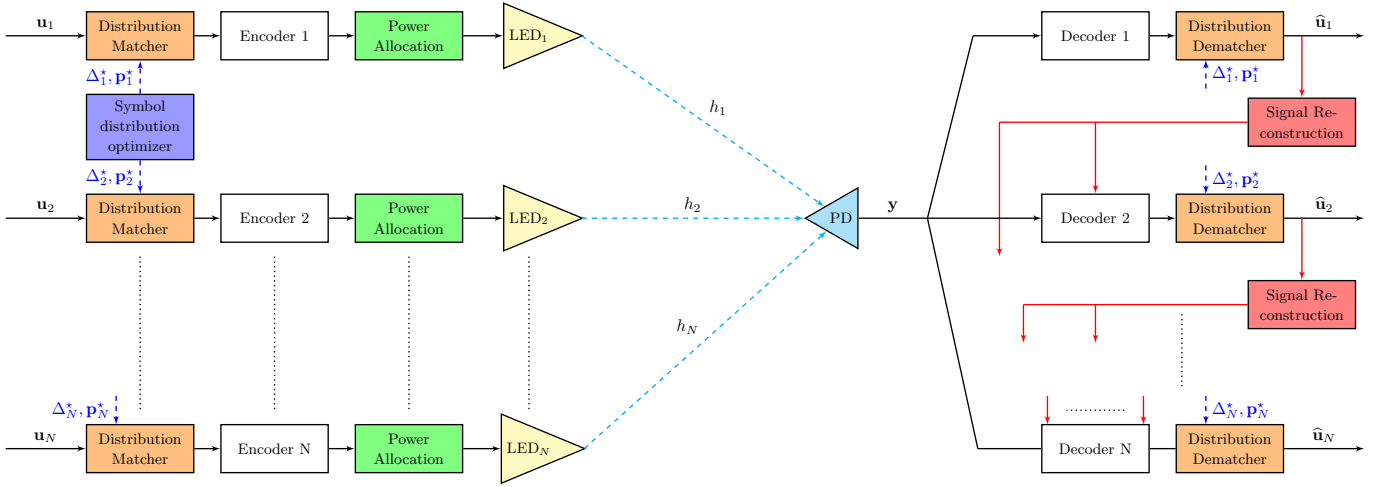


Figure 2: Architecture of NOMA with PS in VLC systems.

TR of our proposed scheme approaches the capacity of NOMA with fine granularity. The main contributions are summarized as follows:

- We propose a novel adaptive coded PS-based NOMA VLC scheme, where the spacing between unipolar M -PAM symbols and their probability mass function (PMF) are optimized for each user depending on the OSNR.
- In contrast to P2P communication, our work incorporates full consideration of multiuser interference to establish the theoretical foundation for derivation of the capacity of uplink NOMA VLC.
- We derive both the AR and TR of the proposed scheme, providing deeper insights into its performance characteristics.
- A multi-variable optimization problem, formulated with the TR objective function, is designed for each user to obtain the optimal distribution of constellation symbols. These optimization problems need to be solved sequentially, following an order that is inverse to the order of SIC.
- Solving optimization problem in original form is intrinsically complex due to the non-convex nature of the original problem. To simplify the problem, we propose an iterative approach where one variable is optimized while the other is fixed alternately.
- The optimization subproblem of alternating iterative approach is still non-convex. To address the non-convexity of optimization subproblem, we introduce a surrogate function, as proposed in [21] and [22], to convexify the subproblem.
- For convexified optimization subproblem, we use Karush-Kuhn-Tucker (KKT) conditions to find the optimal input distribution that approaches the capacity of NOMA.
- We provide an algorithm to compute the capacity-achieving distribution for the proposed scheme.
- The transmission and channel coding rates are adapted to OSNRs.
- We assess the performance of the proposed scheme in terms of SE and frame error rate (FER) under various

conditions of OSNR. Additionally, we compare our results with the lower and upper capacity bounds from [23], as well as with those obtained using PCM, GS, and uniform-distribution schemes.

B. Paper Organization and Notations

The rest of the paper is organized as follows. Section II describes the NOMA VLC system model. The proposed scheme is presented in Section III. In Section IV, we provide the rate analysis for each user. Section V describes optimization problem and proposed algorithm. The performance in terms of the SE and FER are shown in Section VI. Finally, Section VII concludes our work.

This paper uses the following notations. Row vectors and matrices are represented by the lowercase and uppercase bold letters, respectively. The function $(\cdot)^T$ denotes the transpose. The notation $\mathbb{P}\{\cdot\}$ is the probability of an event, while $\mathbb{E}(\cdot)$ is the expectation of a random variable (r.v.). The logarithm function denoted as $\log(\cdot)$ has base two and acts element-wise on vectors. The optimal solution is denoted by $(\cdot)^*$.

II. SYSTEMS MODEL

This section presents the system model for the uplink NOMA transmission scenario. Fig. 1 illustrates the depicted scenario, where N users transmit data to a common photo-detector (PD) at the receiver side. For data transmission, each user is equipped with a single LED. The users are ordered based on their optical channel qualities such that

$$h_1 \leq h_2 \leq \dots \leq h_N, \quad (1)$$

where h_j represents the real-valued gain of the VLC channel between the j -th LED and the PD [24]¹

$$h_j = \begin{cases} \frac{(m+1)A}{2\pi d_j^2} \cos^m(\phi_j) T(\psi_j) G(\psi_j) \cos(\psi_j), & 0 \leq \psi_j \leq \Psi_c \\ 0, & \psi_j > \Psi_c \end{cases}, \quad (2)$$

¹While considering a Line-of-Sight (LOS) path gain akin to [25], our proposed system is versatile and can encompass broader channel characteristics, including Non-Line of Sight (NLOS) links as in [26].

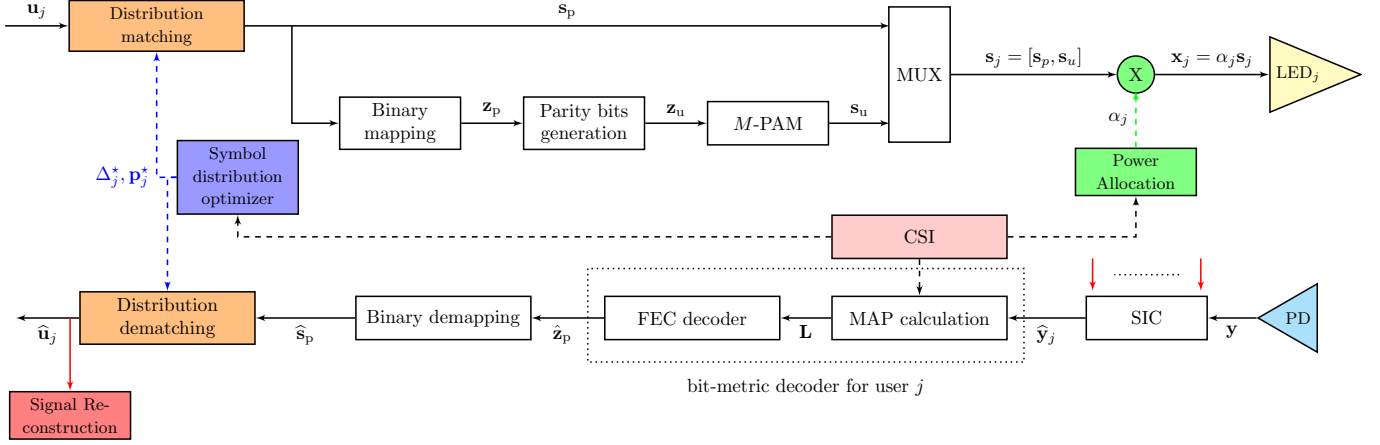


Figure 3: Encoder and decoder for user j of the proposed NOMA VLC scheme with PS.

where d_j denotes the distance from the PD to j -th LED; A and Ψ_c are the area and field-of-view of PD, respectively; ψ_j and ϕ_j are the angles of arrival and departure from j -th LED to the PD with respect to their normal axes, respectively; $T(\psi_j)$ is the gain of the optical filter; $G(\psi_j)$ denotes the gain of the optical concentrator [24]; $\Phi_{1/2}$ is the half-power angle of the LED; and the Lambert's mode number is

$$m = \frac{-\ln(2)}{\ln(\cos(\Phi_{1/2}))}. \quad (3)$$

In the NOMA scheme, the received signal y at the PD is formed by superposition of all signals transmitted from the LEDs in the power domain, i.e.,

$$y = \sum_{j=1}^N h_j x_j + w = \sum_{j=1}^N h_j \alpha_j s_j + w, \quad (4)$$

where $x_j \triangleq \alpha_j s_j$ is the transmitted optical intensity symbol from user j ; $s_j \in \mathcal{S}_j \triangleq \{\Delta_j, 2\Delta_j, \dots, M\Delta_j\}$ is the unipolar M -ary PAM constellation symbol of user j ; Δ_j is the spacing between adjacent symbols of user j ; w is the sum of thermal and high intensity ambient light shot noises, which can be modeled as an additive white Gaussian noise (AWGN) with mean zero and variance σ^2 [26]; and $\alpha_j \triangleq 1/h_j$ is the power allocation weight for the j -th user [24].

Building upon the signal model, we now introduce the constraints that govern the power allocation in the NOMA scheme. To begin, we introduce the notations S_j and X_j as r.v.s representing the constellation and transmitted symbols of user j , respectively. The i -th constellation symbol of user j is denoted as $s_{ji} = \Delta_j i$, where $i \in \mathbb{M} \triangleq \{1, 2, \dots, M\}$, and $x_{ji} \triangleq \alpha_j s_{ji}$. Furthermore, p_j^i is defined as the probability of transmitting the i -th constellation symbol from user j , i.e.,

$$p_j^i \triangleq \mathbb{P}\{S_j = s_{ji}\} = \mathbb{P}\{X_j = x_{ji}\}. \quad (5)$$

Therefore, the average optical transmitted power constraint at user j is

$$\gamma_j \triangleq \alpha_j \sum_{i=1}^M s_{ji} p_j^i = \alpha_j \mathbf{s}_j^T \mathbf{p}_j = \alpha_j P_{rj} \leq P_{\max}, \quad (6)$$

where $\mathbf{p}_j \triangleq [p_j^1, p_j^2, \dots, p_j^M]^T$ is the PMF of S_j ; $s_j \triangleq [s_{j1}, s_{j2}, \dots, s_{jM}]^T$; P_{rj} is a target average optical received power from user j ; and P_{\max} is the maximum average optical transmit power.

From (6), the constellation spacing that satisfies the power constraint is

$$\frac{P_{rj}}{M} \leq \Delta_j \leq P_{rj}. \quad (7)$$

This work utilizes the instantaneous OSNR which is expressed as P_{rj}/σ instead of the electrical signal-to-noise ratio (SNR), as OSNR is more pertinent for VLC systems [27].

In the NOMA system architecture depicted in Fig. 2, the receiver utilizes SIC detection. The decoding order at the receiver is determined based on the average received signal strength, which is influenced by the channel gains. An efficient uplink power control design ensures that the average optical received powers of different users are well separated by allocating larger signal powers to users with lower channel gains [28]. The average optical received power from user j can be expressed as

$$P_{rj} = P_{rN} 10^{\frac{(N-j)c}{10}}, \quad \forall j \in \mathbb{N} \triangleq \{1, 2, \dots, N\}, \quad (8)$$

where

$$c = \frac{10 \log\left(\frac{P_{\max}}{\alpha_1 P_{rN}}\right)}{N-1} \quad (9)$$

is a power back-off coefficient that guarantees the satisfaction of the average optical transmitted power constraint for each user. Additionally, it allows the average optical received power from user j signal to be c -dB weaker than the power from user $(j-1)$ signal, enabling successive mitigation of co-channel interferences.

In NOMA with SIC, the decoding process for user j involves demodulating and decoding signals from users 1 to $j-1$, re-encoding and re-modulating the recovered information bits at the receiver from these users, and subtracting them from the superimposed received signal at user j . The remaining signals from users $j+1$ to N are considered as inter-user interference. To ensure perfect interference cancellation with SIC, the probability of error in detection should be

exceptionally low. This can be achieved by operating within an appropriate AR of the OMAC channel and deploying robust channel coding with an extended code length. Consequently, the received signal at the user j decoder, post SIC processing, can be accurately approximated as

$$\hat{y}_j \triangleq y - \sum_{k=1}^{j-1} h_k x_k = h_j x_j + \sum_{k=j+1}^N h_k x_k + w. \quad (10)$$

III. PROPOSED NOMA VLC SCHEME WITH PS

The proposed NOMA VLC scheme with PS aims to enhance the SE of NOMA VLC systems by probabilistically shaping the distribution of the input symbols and optimizing the constellation spacing. In this section, the proposed encoder and decoder are described.

A. Encoder

The encoder for user j of the proposed scheme is shown in Fig. 3. The encoder transforms information bits into probabilistically shaped channel-coded symbols. In our proposed encoder, a reverse concatenation architecture is used, where the distribution matching is executed before the channel encoding, in order to mitigate the common problem of error bursts when one corrupted symbol at the dematcher input can lead to various corrupted bit-errors at the dematcher output. The proposed encoder consists of several components, including distribution matching (DM), binary mapper, parity bits generator of the FEC encoder, multiplexer, M -PAM converter, symbol distribution optimizer, and LED.

1) *Symbol Distribution Optimizer*: At first, the capacity-achieving distribution of the proposed scheme defined by parameters \mathbf{p}_j^* and Δ_j^* is computed. This distribution allows us to achieve the highest reliable communication rate given a specific OSNR. In Section V, we present an algorithm for obtaining the capacity-achieving distribution.

2) *Distribution Matcher*: In the encoder, an invertible fixed-length DM is used, i.e., CCDM. All possible output sequences of CCDM have an identical target distribution \mathbf{p}_j . In general, the goal of CCDM is to output symbols with distribution \mathbf{p}_j from uniformly distributed stream of input bits. The rate of CCDM is $R_{\text{ccdm}} \triangleq k/n_p$, where k and n_p are the number of input bits and output symbols, respectively. For an output sequence length that tends towards infinity, the CCDM rate converges to the source entropy, i.e.,

$$\lim_{n_p \rightarrow \infty} \frac{k}{n_p} = \mathcal{H}(S_p), \quad (11)$$

where $\mathcal{H}(S_p) = -\sum_{i=1}^M p_j^i \log(p_j^i)$ is the entropy of the discrete r.v. S_p , representing the shaped symbols at the output of CCDM. In case of finite n_p , the CCDM rate is less than the source entropy. However, the rate loss is negligible for a long finite output sequence length [20]. For example, at $n_p = 64800$, the rate loss is less than 7.5×10^{-4} bits/symbol for 8-PAM [29].

In our proposed encoder, the CCDM transforms uniformly distributed stream of information bits, $\mathbf{u}_j \in \{0, 1\}^k$, into

probabilistically shaped unipolar M -PAM symbols represented by $\mathbf{s}_p \in \{\Delta_j^*, 2\Delta_j^*, \dots, M\Delta_j^*\}^{n_p}$ with the target distribution \mathbf{p}_j^* , which is computed in Section V.

3) *Channel Encoder*: Binary FEC encoder is being used to achieve reliable communication with a data rate that is close to the channel capacity. The probabilistically shaped M -PAM symbols, $\mathbf{s}_p \triangleq [s_p^1, s_p^2, \dots, s_p^{n_p}]$, are converted into a vector of bits, $\mathbf{z}_p \in \{0, 1\}^{\log(M) n_p}$, using the binary mapper such that

$$\mathbf{z}_p \triangleq [\mathbb{B}(s_p^1), \mathbb{B}(s_p^2), \dots, \mathbb{B}(s_p^{n_p})], \quad (12)$$

where

$$\mathbb{B}(s_p^k) \triangleq [b_1^k, b_2^k, \dots, b_{\log(M)}^k], \text{ for } k \in \{1, 2, \dots, n_p\}, \quad (13)$$

and b_l^k is the bit level l of the symbol s_p^k . We use Gray code binary mapper, as it yields good performance [10].

Then, the bits are coded with the systematic binary FEC encoder with a channel coding rate R_{FEC} as

$$\mathbf{z}_u^T = \mathbf{C} \mathbf{z}_p^T, \quad (14)$$

where $\mathbf{C} \in \{0, 1\}^{\left(\frac{1}{R_{\text{FEC}}} - 1\right) n_p \log(M) \times n_p \log(M)}$ is the parity matrix, which can be obtained by representing the code generator matrix in a standard form [30]. Please note that, regardless of the distribution of \mathbf{z}_p , the parity bits, $\mathbf{z}_u \in \{0, 1\}^{\left(\frac{1}{R_{\text{FEC}}} - 1\right) n_p \log(M)}$, are approximately uniformly distributed. The reason is that when a large number of bits are added, the distribution of the resulting bits tends to be uniform, even if the distribution of the original bits is not uniform [31].

4) *Sparse-Dense Signal*: The uniformly distributed unipolar M -PAM symbols, $\mathbf{s}_u \in \{\Delta_j^*, 2\Delta_j^*, \dots, M\Delta_j^*\}^{\left(\frac{1}{R_{\text{FEC}}} - 1\right) n_p}$, are produced from the parity bits, \mathbf{z}_u , using the binary demapper. After that, the multiplexer appends probabilistically shaped and uniformly distributed symbols to form a codeword consisting of $n = n_p/R_{\text{FEC}}$ symbols, such that

$$\mathbf{s}_j = [\mathbf{s}_p, \mathbf{s}_u]. \quad (15)$$

Consequently, the codeword in (15) is multiplied by the power allocation coefficient α_j to form the transmitted signal, i.e.,

$$\mathbf{x}_j = \alpha_j \mathbf{s}_j. \quad (16)$$

The signal in (16) is a sparse-dense transmission (SDT) signal because uniformly distributed symbols have the maximum source entropy (representing dense information), while the probabilistically shaped symbols represent smaller entropy (representing sparse information).

B. Decoder

After discussing the proposed encoder and its output in the previous subsection, our attention now shifts to the decoder for user j within the proposed scheme, as illustrated in Fig. 3. The objective is to achieve the maximum AR of the SDT signal by employing the optimal symbol metric decoder (SMD) for FEC decoding. However, it is worth noting that SMD entails high computational complexity [10]. Therefore, to strike a balance between computational complexity and achieving a rate close to the SDT capacity, we propose the utilization of bit

metric decoder (BMD) with soft decision-making capabilities. This approach involves calculating the maximum a posteriori probability (MAP) for each bit level of every received symbol. The selection of MAP is motivated by its incorporation of prior knowledge, including the probability distribution of the transmitted symbols. In contrast, maximum likelihood (ML) decoding relies solely on the received signal and assumes a uniform distribution of the transmitted symbols.

1) *SIC*: As can be seen from Fig. 3, the received signal y at the PD is the input to SIC block. After applying SIC as described in (10), the output of SIC block is $\hat{y}_j \triangleq [\hat{y}_j^1, \hat{y}_j^2, \dots, \hat{y}_j^n]$, where \hat{y}_j^t is the received signal at the decoder of user j at time instant $t \in \{1, 2, \dots, n\}$.

2) *MAP Calculation*: Let us consider the M -PAM symbol transmitted by user j at time instant t , denoted by x_j^t . It consists of individual bit levels represented by r.v.s $B_{j,l}^t \in \{0, 1\}$, where l denotes the bit level. Therefore, its binary representation is

$$\mathbb{B}(x_j^t) = [B_{j,1}^t, B_{j,2}^t, \dots, B_{j,\log(M)}^t]. \quad (17)$$

The r.v.s representing x_j^t and \hat{y}_j^t are X_j^t and \hat{Y}_j^t , respectively. Therefore, the MAP of the l th bit level given \hat{y}_j^t is

$$\begin{aligned} L_{t,l}^j &= \log \left(\frac{f_{B_{j,l}^t|\hat{Y}_j^t}(0|\hat{y}_j^t)}{f_{B_{j,l}^t|\hat{Y}_j^t}(1|\hat{y}_j^t)} \right) \\ &= \log \left(\frac{\sum_{x_j \in \mathbb{X}_l^0} f_{\hat{Y}_j^t|X_j^t}(\hat{y}_j^t|x) \mathbb{P}\{X_j^t = x_j\}}{\sum_{x_j \in \mathbb{X}_l^1} f_{\hat{Y}_j^t|X_j^t}(\hat{y}_j^t|x) \mathbb{P}\{X_j^t = x_j\}} \right), \quad (18) \end{aligned}$$

where \mathbb{X}_l^0 and \mathbb{X}_l^1 are the sets containing all the values of x_j whose l th bit level is 0 and 1, respectively. Please note that, in SDT signal, the distribution of X_j^t depends on t . Hence, for $t \in \{nR_{\text{FEC}} + 1, nR_{\text{FEC}} + 2, \dots, n\}$, $\mathbb{P}\{X_j^t = x_j\} = 1/M$.

3) *FEC Decoder and Dematcher*: Since $L_{t,l}^j$ serves as the sufficient statistic for estimating the bit level l based on the received symbol \hat{y}_j^t [10], the FEC soft decoder takes MAP values obtained in (18) as input for error correction. Consequently, the output of the FEC soft decoder is denoted as $\hat{z}_p \in \{0, 1\}^{\log(M)n_p}$. Following this, the corresponding unipolar M -PAM symbols, $\hat{s}_p \in \{\Delta_j^*, 2\Delta_j^*, \dots, M\Delta_j^*\}^{n_p}$, are obtained from \hat{z}_p using a binary demapper. Lastly, the distribution dematching process maps the symbols from \hat{s}_p to the corresponding recovered information bits of user j , denoted as $\hat{u}_j \in \{0, 1\}^k$, which are subsequently re-encoded and re-modulated for utilization in SIC operations.

IV. RATE ANALYSIS

To find the capacity-achieving distribution of the proposed scheme, we need to derive its AR and TR. AR of the proposed scheme is derived accounting for *i*) constraints imposed by the intensity modulation and direct detection (IM/DD) such as non-negative and real-valued input signal; *ii*) NOMA features such as OMAC properties and employment of the SIC detection; *iii*) the SDT signalling in (16), where only part of the transmitted symbols can be probabilistically shaped.

A. Achievable Rate of the Proposed Scheme

In this subsection, we derive the AR of the proposed scheme. Let \hat{Y}_j be a r.v. representing the received signal in (10). According to the SIC decoding principle in NOMA, the received signal at the decoder of user j (i.e., \hat{y}_j) includes interference signals from users $j+1$ to N , which have constellation spacing values denoted by $\bar{\Delta}_{j+1} \triangleq [\Delta_{j+1}, \Delta_{j+2}, \dots, \Delta_N]$ and follow PMFs denoted by $\bar{\mathbf{p}}_{j+1} \triangleq [\mathbf{p}_{j+1}^T, \mathbf{p}_{j+2}^T, \dots, \mathbf{p}_N^T]$, respectively. We use $\mathbf{a}_{\hat{y}_j} \triangleq [\bar{\Delta}_{j+1}, \bar{\mathbf{p}}_{j+1}]$ to represent the spacing values and PMFs of the interference signals in \hat{y}_j .

An AR of user j of the proposed scheme is

$$\begin{aligned} R_j^{\text{SDT}}(\Delta_j, \mathbf{p}_j, \mathbf{a}_{\hat{y}_j}) &\triangleq R_{\text{FEC}} R_j(\Delta_j, \mathbf{p}_j, \mathbf{a}_{\hat{y}_j}) \\ &\quad + (1 - R_{\text{FEC}}) R_j(\Delta_j, \mathbf{p}_j^u, \mathbf{a}_{\hat{y}_j}), \quad (19) \end{aligned}$$

where $\mathbf{p}_j^u \triangleq [1/M, 1/M, \dots, 1/M]^T$ and

$$\begin{aligned} R_j(\Delta_j, \mathbf{p}_j, \mathbf{a}_{\hat{y}_j}) &= \mathcal{I}(X_j; \hat{Y}_j) \\ &= \mathcal{H}(X_j) - \mathcal{H}(X_j|\hat{Y}_j) \\ &= -\sum_{i=1}^M p_j^i \log(p_j^i) - \mathcal{H}(X_j|\hat{Y}_j), \quad (20) \end{aligned}$$

where $\mathcal{I}(X_j; \hat{Y}_j)$ represents the mutual information (MI) between transmitted signal X_j and received signal \hat{Y}_j , $\mathcal{H}(X_j)$ is the entropy of the r.v. X_j , and $\mathcal{H}(X_j|\hat{Y}_j)$ is the conditional entropy, which can be derived as

$$\begin{aligned} \mathcal{H}(X_j|\hat{Y}_j) &= -\int_{-\infty}^{\infty} f_{\hat{Y}_j}(\hat{y}_j) \sum_{i=1}^M f_{X_j|\hat{Y}_j}(s_{ji}|\hat{y}_j) \log(f_{X_j|\hat{Y}_j}(s_{ji}|\hat{y}_j)) d\hat{y}_j \\ &= -\int_{-\infty}^{\infty} f_{\hat{Y}_j}(\hat{y}_j) \sum_{i=1}^M \frac{f_{\hat{Y}_j|X_j}(\hat{y}_j|s_{ji}) f_{X_j}(s_{ji})}{f_{\hat{Y}_j}(\hat{y}_j)} \\ &\quad \times \log \left(\frac{f_{\hat{Y}_j|X_j}(\hat{y}_j|s_{ji}) f_{X_j}(s_{ji})}{f_{\hat{Y}_j}(\hat{y}_j)} \right) d\hat{y}_j \\ &= -\int_{-\infty}^{\infty} \sum_{i=1}^M f_{\hat{Y}_j|X_j}(\hat{y}_j|s_{ji}) f_{X_j}(s_{ji}) \\ &\quad \times \log \left(\frac{f_{\hat{Y}_j|X_j}(\hat{y}_j|s_{ji}) f_{X_j}(s_{ji})}{f_{\hat{Y}_j}(\hat{y}_j)} \right) d\hat{y}_j \\ &= \int_{-\infty}^{\infty} \sum_{i=1}^M f_{\hat{Y}_j|X_j}(\hat{y}_j|s_{ji}) f_{X_j}(s_{ji}) \\ &\quad \times \log \left(\frac{f_{\hat{Y}_j}(\hat{y}_j)}{f_{\hat{Y}_j|X_j}(\hat{y}_j|s_{ji}) f_{X_j}(s_{ji})} \right) d\hat{y}_j, \quad (21) \end{aligned}$$

where

$$f_{\hat{Y}_j|X_j}(\hat{y}_j|s_{ji}) = \sum_{\{s_k\}_{k=j+1}^N \in \{\mathcal{S}_k\}_{k=j+1}^N} f_{\hat{Y}_j|\{X_k\}_{k=j}^N}(\hat{y}_j|s_{ji}, \{s_k\}_{k=j+1}^N) \prod_{k=j+1}^N f_{X_k}(s_k)$$

$$= \sum_{\{s_k\}_{k=j+1}^N \in \{\mathcal{S}_k\}_{k=j+1}^N} \frac{e^{-\left(\frac{\hat{y}_j - h_j \alpha_j s_{ji} - \sum_{k=j+1}^N h_k \alpha_k s_k}{2\sigma^2}\right)^2}}{\sqrt{2\pi\sigma^2}} \prod_{k=j+1}^N f_{X_k}(s_k), \quad (22)$$

and where

$$f_{\hat{Y}_j}(\hat{y}_j) = \sum_{i'=1}^M f_{\hat{Y}_j|X_j}(\hat{y}_j|s_{ji'}) f_{X_j}(s_{ji'}), \quad (23)$$

$$f_{X_j}(s_{ji}) = p_j^i. \quad (24)$$

Note that $R_j(\Delta_j, \mathbf{p}_j, \mathbf{a}_{\hat{y}_j}^*)$ is the AR of user j for NOMA with IM/DD, where all of the transmitted symbols can be probabilistically shaped.

B. Transmission Rate of the Proposed Scheme

We now shift our focus to deriving the TR achieved by the proposed scheme. The TR is defined as a fraction of information bits over the number of channel uses. The TR of user j for the proposed scheme shown in Fig. 3 can be derived as

$$T_j(\mathbf{p}_j) \triangleq \frac{k}{n} = \frac{n_p \mathcal{H}(S_p)}{n} = -R_{\text{FEC}} \sum_{i=1}^M p_j^i \log(p_j^i), \quad (25)$$

where k is the number of information bits, and n is the frame size. Note that the following condition $T_j \leq R_j^{\text{SDT}}$ should be satisfied in order to guarantee reliable communication. When this condition is satisfied, the TR of the proposed scheme is achievable.

V. RATE ADAPTATION

The TR of the proposed scheme for user j can be adapted by adjusting the distribution of unipolar M -PAM symbols, denoted as \mathbf{p}_j , and the channel coding rate, denoted as R_{FEC} . In this section, we propose an algorithm to maximize the achievable TR by optimizing \mathbf{p}_j and Δ_j for given OSNR and R_{FEC} .

A. Optimization Problem

In this subsection, we delve into the rate adaptation problem by presenting an optimization problem that allows us to mathematically formulate and seek the optimal \mathbf{p}_j and Δ_j . To determine the TR of each user, it is necessary to jointly optimize \mathbf{p}_j and Δ_j for every user. Consequently, there are N separate optimization problems that need to be solved sequentially.

Considering the power and rate constraints, the maximum achievable TR of user j of the proposed scheme for the given R_{FEC} and OSNR can be obtained from

$$\text{maximize}_{\Delta_j, \mathbf{p}_j} T_j(\mathbf{p}_j) \quad (26a)$$

$$\text{subject to } R_{\text{FEC}} \mathbf{s}_j^T \mathbf{p}_j + (1 - R_{\text{FEC}}) \mathbf{s}_j^T \mathbf{p}_j^u = P_{rj}, \quad (26b)$$

$$T_j(\mathbf{p}_j) \leq R_j^{\text{SDT}}(\Delta_j, \mathbf{p}_j, \mathbf{a}_{\hat{y}_j}^*) - R_{\text{bf}}, \quad (26c)$$

$$\Delta_{j,\min} \leq \Delta_j \leq \Delta_{j,\max}, \quad (26d)$$

$$\sum_{i=1}^M p_j^i = 1, \quad (26e)$$

$$p_j^i \geq 0, \quad \forall i \in \mathbb{M}, \quad (26f)$$

where $\mathbf{a}_{\hat{y}_j}^* \triangleq [\underline{\Delta}_{j+1}^*, \bar{\mathbf{P}}_{j+1}^*]$, R_{bf} is the back-off rate to compensate the rate loss due to the use of BMD and finite-length distribution matcher and

$$\Delta_{j,\min} \triangleq \frac{P_{rj}}{(R_{\text{FEC}}M + (1 - R_{\text{FEC}}) \frac{M+1}{2})}, \quad (27)$$

$$\Delta_{j,\max} \triangleq \frac{P_{rj}}{(R_{\text{FEC}} + (1 - R_{\text{FEC}}) \frac{M+1}{2})}. \quad (28)$$

The constraint (26b) ensures that the total power, taking into account the coding rate and symbol distribution, is equal to the received power. The minimum and maximum symbol spacings, denoted as $\Delta_{j,\min}$ and $\Delta_{j,\max}$, are derived based on the power allocation and coding rate to satisfy the power constraint. The constraint (26c) guarantees reliable communication with an achievable TR.

In NOMA with SIC, the decoding order starts from user 1 and ends at user N . The received signal of the last decoded user is given by $\hat{y}_N = h_N x_N + w$, where there is no interference from other users. For the received signal of the prior decoded user (i.e., $\hat{y}_{j < N}$), we observe the presence of interference from both AWGN and multiuser interference from users $j+1$ to N . To ensure optimal distribution of the user $j < N$ signal, it is essential to account for this inter-user interference. Therefore, the order of optimization is opposite to the SIC decoding order, which means that the optimization problem (26) is solved starting from user N and then progressing backward to user 1. For example, we first find \mathbf{p}_N^* and Δ_N^* for user N from (26), where $\mathbf{a}_{\hat{y}_N}^*$ is an empty vector. Next, we obtain \mathbf{p}_{N-1}^* and Δ_{N-1}^* for user $N-1$ from (26), taking into account the interference signal from user N in \hat{y}_{N-1} , which follows the distribution given by \mathbf{p}_N^* and has constellation spacing Δ_N^* , i.e., $\mathbf{a}_{\hat{y}_{N-1}}^* = [\Delta_N^*, \mathbf{p}_N^{*T}]$. We continue this process to obtain the optimal PMF and spacing for the remaining users in accordance with the optimization order.

B. Proposed Algorithm

This subsection proposes an algorithm to efficiently find the capacity-approaching distribution of the proposed scheme. Optimizing \mathbf{p}_j and Δ_j jointly in (26) is excessively complex non-convex problem. Therefore, we propose an iterative approach where one variable is optimized while the other is fixed alternately. Nevertheless, optimizing \mathbf{p}_j while fixing Δ_j

results in the non-convexity of the optimization problem due to (26c). To address this challenge, we employ a surrogate function, a mathematical construct designed to approximate the original non-convex objective function with a convex counterpart, inspired by the work of [22]. This surrogate function plays a crucial role in convexifying our problem, allowing the algorithm to iteratively approach the optimized solution. With each iteration, our approach converges toward a solution that balances computational efficiency and optimality. In this regard, $R_j^{\text{SDT}}(\Delta_j, \mathbf{p}_j, \mathbf{a}_{\hat{y}_j}^*)$ can be rewritten as

$$R_j^{\text{SDT}}(\Delta_j, \mathbf{p}_j, \mathbf{a}_{\hat{y}_j}^*) = R_{\text{FEC}} \left(g_1(\mathbf{p}_j) - g_2(\Delta_j, \mathbf{p}_j, \mathbf{a}_{\hat{y}_j}^*) \right) + (1 - R_{\text{FEC}}) R_j(\Delta_j, \mathbf{p}_j^u, \mathbf{a}_{\hat{y}_j}^*), \quad (29)$$

where

$$g_1(\mathbf{p}_j) \triangleq - \sum_{i=1}^M p_j^i \log(p_j^i), \quad (30)$$

$$g_2(\Delta_j, \mathbf{p}_j, \mathbf{a}_{\hat{y}_j}^*) \triangleq \sum_{i=1}^M p_j^i W(i, \Delta_j, \mathbf{p}_j, \mathbf{a}_{\hat{y}_j}^*), \quad (31)$$

and

$$W(i, \Delta_j, \mathbf{p}_j, \mathbf{a}_{\hat{y}_j}^*) \triangleq \int_{-\infty}^{\infty} f_{\hat{Y}_j|X_j}(\hat{y}_j | s_{ji}) \times \log\left(\frac{f_{\hat{Y}_j}(\hat{y}_j)}{f_{\hat{Y}_j|X_j}(\hat{y}_j | s_{ji}) p_j^i}\right) d\hat{y}_j. \quad (32)$$

Optimizing R_j^{SDT} with respect to \mathbf{p}_j is complex and results in a coupling problem because the function (31) cannot be represented as a linear summation of concave functions with optimization variables p_j^i . Thus, we introduce the surrogate function, $\Phi(\mathbf{p}_j, \hat{\mathbf{p}}_j)$, which can be used to approximate R_j^{SDT} around $\mathbf{p}_j = \hat{\mathbf{p}}_j$, i.e.,

$$\Phi(\mathbf{p}_j, \hat{\mathbf{p}}_j) \triangleq R_{\text{FEC}} \left(g_1(\mathbf{p}_j) - g_2'(\Delta_j, \mathbf{p}_j, \hat{\mathbf{p}}_j, \mathbf{a}_{\hat{y}_j}^*) \right) + (1 - R_{\text{FEC}}) R_j(\Delta_j, \mathbf{p}_j^u, \mathbf{a}_{\hat{y}_j}^*), \quad (33)$$

where

$$g_2'(\Delta_j, \mathbf{p}_j, \hat{\mathbf{p}}_j, \mathbf{a}_{\hat{y}_j}^*) \triangleq \sum_{i=1}^M p_j^i W(i, \Delta_j, \hat{\mathbf{p}}_j, \mathbf{a}_{\hat{y}_j}^*). \quad (34)$$

According to the relative entropy properties [22], if $\hat{\mathbf{p}}_j = \mathbf{p}_j$, then $g_2'(\Delta_j, \mathbf{p}_j, \hat{\mathbf{p}}_j, \mathbf{a}_{\hat{y}_j}^*) = g_2(\Delta_j, \mathbf{p}_j, \mathbf{a}_{\hat{y}_j}^*)$, otherwise $g_2'(\Delta_j, \mathbf{p}_j, \hat{\mathbf{p}}_j, \mathbf{a}_{\hat{y}_j}^*) > g_2(\Delta_j, \mathbf{p}_j, \mathbf{a}_{\hat{y}_j}^*)$. Thus, given R_{FEC} , R_{bf} , initial PMF $\hat{\mathbf{p}}_j$, and OSNR, the convexified version of (26) for fixed Δ_j is

$$\mathbf{p}_{\Delta_j}^* = \underset{\mathbf{p}_j}{\text{maximize}} \quad T_j(\mathbf{p}_j) \quad (35a)$$

$$\text{subject to} \quad R_{\text{FEC}} \mathbf{s}_j^T \mathbf{p}_j + (1 - R_{\text{FEC}}) \mathbf{s}_j^T \mathbf{p}_j^u = P_{rj}, \quad (35b)$$

$$T_j(\mathbf{p}_j) \leq \Phi(\mathbf{p}_j, \hat{\mathbf{p}}_j) - R_{\text{bf}}, \quad (35c)$$

$$\sum_{i=1}^M p_j^i = 1, \quad (35d)$$

$$p_j^i \geq 0, \quad \forall i \in \mathbb{M}. \quad (35e)$$

Since $\Phi(\mathbf{p}_j, \hat{\mathbf{p}}_j) \leq \Phi(\mathbf{p}_j, \mathbf{p}_j) = R_j^{\text{SDT}}(\Delta_j, \mathbf{p}_j, \mathbf{a}_{\hat{y}_j}^*)$, the constraint (26c) is not violated by (35c).

We use KKT optimality conditions to solve the convex optimization problem (35). The Lagrangian function can be expressed as

$$L = -T_j(\mathbf{p}_j) + \mu \left(\sum_{i=1}^M p_j^i - 1 \right) + \eta \left(R_{\text{FEC}} \sum_{i=1}^M \Delta_j p_j^i - P_j \right) + \tau (T_j(\mathbf{p}_j) - \Phi(\mathbf{p}_j, \hat{\mathbf{p}}_j) + R_{\text{bf}}), \quad (36)$$

where $P_j \triangleq P_{rj} - (1 - R_{\text{FEC}}) \mathbf{s}_j^T \mathbf{p}_j^u$, and the Lagrangian multipliers are denoted as μ , η and τ . The solution to (35) using KKT optimality conditions is shown in the following lemma

Lemma V.1 (KKT solution to (35)). *For the given Δ_j , R_{FEC} , $\hat{\mathbf{p}}_j$, and OSNR,*

$$p_{\Delta_j}^{*i} = \begin{cases} \frac{2^{-\eta \Delta_j i}}{\sum_{i'=1}^M 2^{-\eta \Delta_j i'}} & \text{if } c_1^p \text{ and } c_1^r \text{ are satisfied} \\ \frac{2^{-\eta \Delta_j i - \tau W(i, \Delta_j, \hat{\mathbf{p}}_j, \mathbf{a}_{\hat{y}_j}^*)}}{\sum_{i'=1}^M 2^{-\eta \Delta_j i' - \tau W(i', \Delta_j, \hat{\mathbf{p}}_j, \mathbf{a}_{\hat{y}_j}^*)}} & \text{if } c_2^p \text{ and } c_2^r \text{ are satisfied,} \end{cases} \quad (37)$$

where

$$c_1^p \triangleq \sum_{i'=1}^M (R_{\text{FEC}} \Delta_j i - P_j) 2^{-\eta \Delta_j i} = 0, \quad (38)$$

$$c_1^r \triangleq \sum_{i=1}^M \left[R_{\text{FEC}} W(i, \Delta_j, \hat{\mathbf{p}}_j, \mathbf{a}_{\hat{y}_j}^*) - D \right] 2^{-\eta \Delta_j i} < 0, \quad (39)$$

$$c_2^p \triangleq \sum_{i'=1}^M (R_{\text{FEC}} \Delta_j i - P_j) 2^{-\eta \Delta_j i - \tau W(i, \Delta_j, \hat{\mathbf{p}}_j, \mathbf{a}_{\hat{y}_j}^*)} = 0, \quad (40)$$

and

$$c_2^r \triangleq \sum_{i=1}^M \left[R_{\text{FEC}} W(i, \Delta_j, \hat{\mathbf{p}}_j, \mathbf{a}_{\hat{y}_j}^*) - D \right] \frac{2^{-\eta \Delta_j i}}{2^{\tau W(i, \Delta_j, \hat{\mathbf{p}}_j, \mathbf{a}_{\hat{y}_j}^*)}} = 0, \quad (41)$$

where $D = (1 - R_{\text{FEC}}) R_j(\Delta_j, \mathbf{p}_j^u, \mathbf{a}_{\hat{y}_j}^*) - R_{\text{bf}}$, τ and η are any positive real numbers.

Proof. The detailed derivation is shown in Appendix B. \square

The proposed algorithm leverages Lemma V.1 to efficiently find optimal PMF of user j for the given Δ_j , i.e., $\mathbf{p}_{\Delta_j}^*$. The algorithm updates $\hat{\mathbf{p}}_j$ in each iteration by computing the new distribution vector $\mathbf{p}_{\Delta_j}^*$ and calculating the distance between $\hat{\mathbf{p}}_j$ and $\mathbf{p}_{\Delta_j}^*$. The iteration continues until the distance falls below the threshold γ_s , indicating convergence. Finally, the algorithm outputs the optimal distribution vector $\mathbf{p}_{\Delta_j}^*$.

To determine the optimized constellation spacing, Δ_j^* , that maximizes $R_j^{\text{SDT}}(\Delta_j, \mathbf{p}_j, \mathbf{a}_{\hat{y}_j}^*)$ for fixed \mathbf{p}_j , we employ the golden section method. The range of search for Δ_j is specified in (26d). Algorithm 1 and golden section method are iterated for each of the FEC coding rates of a low-density parity-check

Algorithm 1 Proposed algorithm to find optimal \mathbf{p}_j in (35)

- 1: **Inputs:** Δ_j , R_{FEC} , σ , R_{bf} , and $\gamma_s > 0$ % γ_s is the stopping threshold
 - 2: **Initialize:** vector $\hat{\mathbf{p}}_j$ which satisfies constraints in (35)
 - 3: **repeat**
 - 4: **Step 1:** For each $i \in \{1, 2, \dots, M\}$,
 compute $W(i, \Delta_j, \hat{\mathbf{p}}_j, \mathbf{a}_{\hat{y}_j}^*)$
 - 5: **Step 2:** Obtain new distribution vector $\mathbf{p}_{\Delta_j}^*$ from Lemma V.1
 - 6: **Step 3:** $\epsilon = \|\hat{\mathbf{p}}_j - \mathbf{p}_{\Delta_j}^*\|^2$
 - 7: **Update:** $\hat{\mathbf{p}}_j := \mathbf{p}_{\Delta_j}^*$
 - 8: **until** $\epsilon < \gamma_s$
 - 9: **Output:** $\mathbf{p}_{\Delta_j}^*$
-

Table II: Convergence of Algorithm 1

M	v_p : Number of Iterations until convergence
2	1
4	6
8	26
16	403
64	512

(LDPC) channel encoder in a DVB-S2 receiver [29]. For a given OSNR, the optimal FEC coding rate, R_{FEC}^* , is the one which results in the highest achievable TR.

C. Computational Complexity

This subsection analyzes the computational complexity of the proposed scheme. The major portion of the computational complexity results from solving the optimization problem to get the capacity-achieving distribution.

The proposed approach adopts an iterative alternate optimization method, necessitating the execution of Algorithm 1 for each constellation spacing value. We denote v_p as the number of iterations required to meet the convergence criteria in Algorithm 1. As shown in Table II, v_p exhibits an approximately linear increase with the constellation size M . Additionally, v_Δ represents the number of iterations required to converge to the optimal constellation spacing value in the golden section algorithm.

Furthermore, we define v_{fec} as the number of coding rates accommodated by the FEC encoder for the given M -ary modulation. Consequently, finding the optimal parameters for N users with a specific OSNR necessitates solving $Nv_p v_\Delta v_{fec}$ convex optimization problems. The computational complexity of finding a solution to a single convex optimization problem for an M -ary modulation, employing the interior-point method, scales as $\mathcal{O}(M^3)$ [32].

The optimization process can be carried out either online or offline, considering the computational resources available at the transmitting side. Offline optimization involves obtaining the optimal constellation size, FEC rate, symbol distribution and constellation spacing for a predefined set of OSNRs. These optimized parameters are then stored in memory, which reduces the computational complexity during transmission.

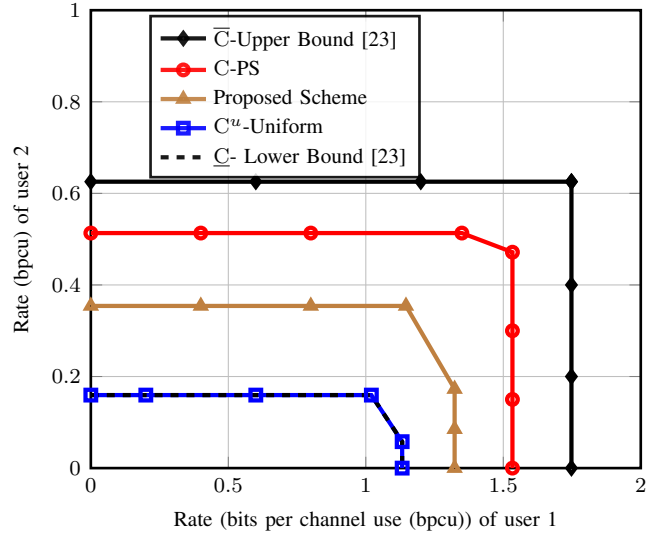


Figure 4: Capacity region of NOMA for $M = 8$ and at OSNR $P_{r1}/\sigma = 6$ dB.

However, the discretization process may result in some rate loss.

VI. NUMERICAL RESULTS

In this section, we present numerical results to evaluate the performance of our proposed scheme in terms of SE and FER considering two users, i.e., $N = 2$. FER is chosen as the performance metric instead of BER because FER is considered to be a more robust metric than BER [10]. Channel coding is performed using LDPC codes specified in DVB-S2 [29]. The block length used for all codes in DVB-S2 is fixed at 64800 bits. The optimal parameters such as distribution, constellation spacing, and FEC rate are determined by Algorithm 1 outlined in Section V with $R_{\text{bf}} = 0.05$. Without loss of generality, the received OSNR is defined as P_{r1}/σ in (dB) units.

The main performance benchmarks are as follows:

- Upper bound on the capacity of OMAC channel denoted as \bar{C}_j and proposed in [23].
- Capacity of NOMA denoted as C_j , which is the maximum of power-constrained $R_j(\Delta_j, \mathbf{p}_j, \mathbf{a}_{\hat{y}_j}^*)$ for all feasible input distributions. The calculation of C_j is shown in Appendix A.
- Uniform-distribution scheme, where output symbols of DM and symbols resulted from the parity bits have uniform distribution.
- PCM scheme proposed in [33] and extended to NOMA case. In the PCM scheme, the output symbols of DM have

Table III: Performance gains of the proposed scheme.

Transmission Rate	User 1 Gap (dB)	User 2 Gap (dB)
0.75	1.3	2
1	0.5	1.5
2	0.5	0.9
2.5	0	0

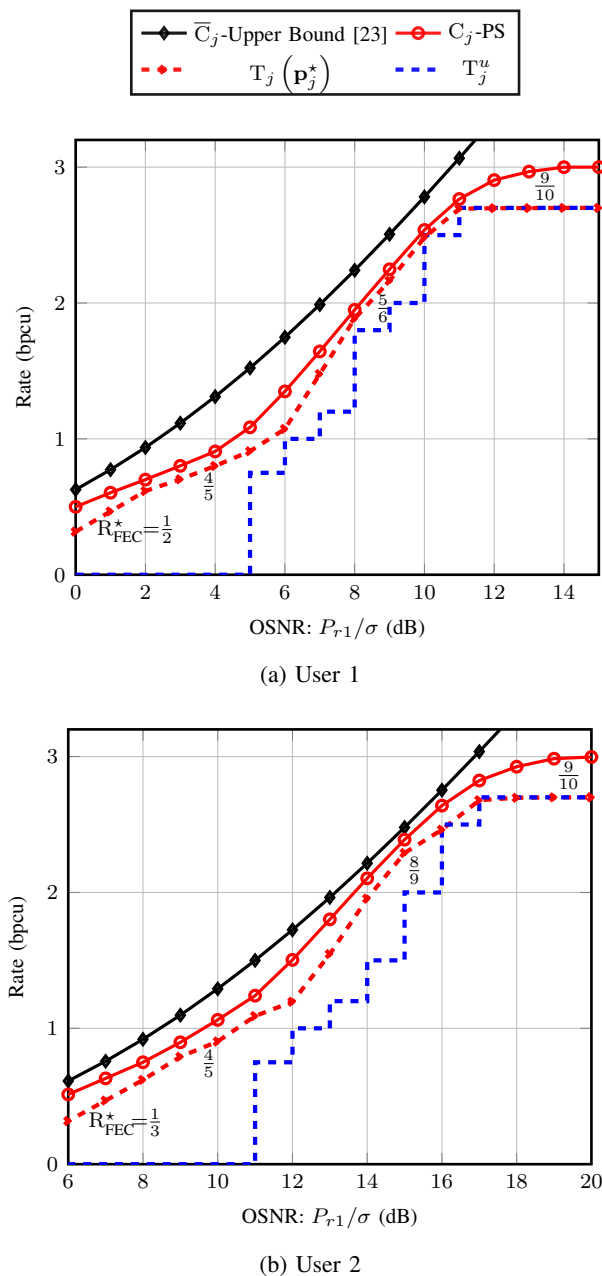


Figure 5: Transmission rates vs OSNR for $M = 8$.

an optimized pairwise distribution with equal probabilities for two consecutive constellation symbols while the symbols resulted from the parity bits remain uniformly distributed.

- GS scheme, where the spacing values between constellation symbols are optimized while maintaining a uniform distribution.

In Fig. 4, we present the capacity region characteristics in the NOMA VLC system for $M = 8$ at OSNR $P_{r1}/\sigma = 6$ dB. The capacity region of NOMA, denoted as C , is separated from the theoretical upper bound on the capacity of the OMAC channel, denoted as \bar{C} , by a maximum gap of 0.2 bpcu. The maximum AR region of the proposed scheme exhibits an improvement of approximately 0.2 bpcu over the capacity

region of the uniform-distribution scheme, denoted as C^u . The lower bound on the capacity region of the OMAC channel, denoted as \underline{C} , coincides with C^u since they both utilize a uniform distribution. As a result, C^u is regarded as a lower bound for the remainder of this section.

Fig. 5 illustrates the capacity of NOMA, C_j , its upper bound, \bar{C}_j , TR of the proposed scheme, T_j , and TR of the uniform-distribution scheme, T_j^u , as a function of OSNR for user j and $M = 8$. The optimal FEC coding rate, R_{FEC}^* , is adaptively adjusted based on the OSNR for each user. The achieved performance gains of the proposed scheme, in terms of OSNR, compared to the uniform-distribution scheme for different TRs of both users are summarized in Table III. As

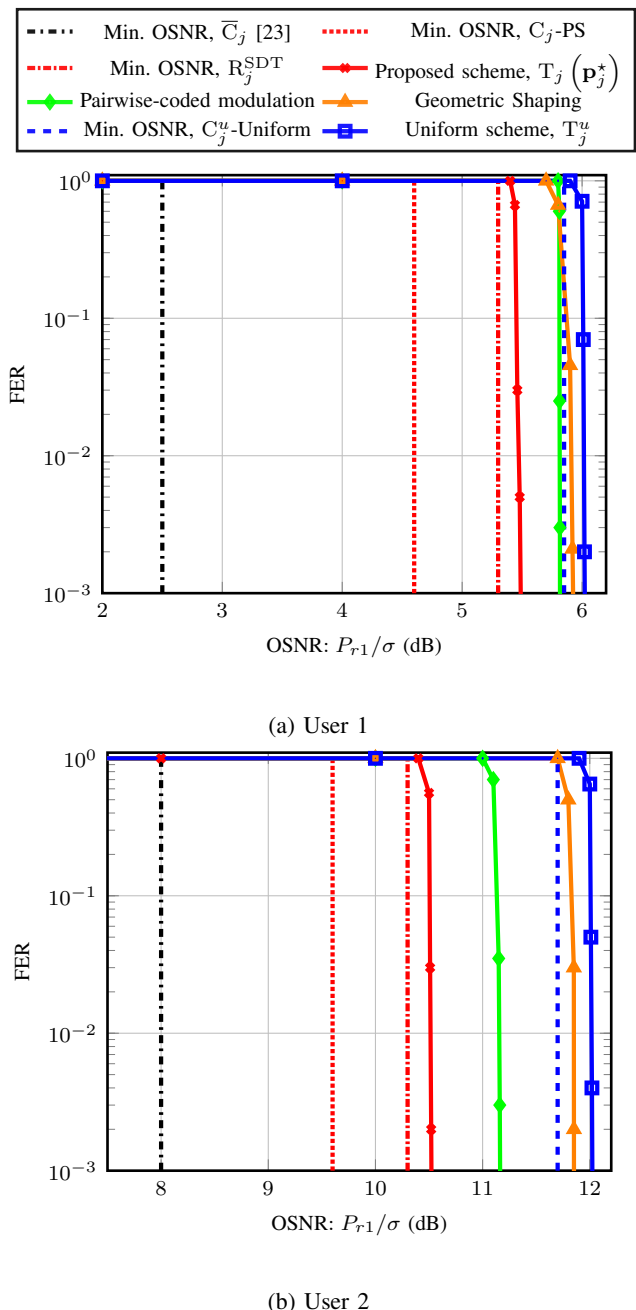
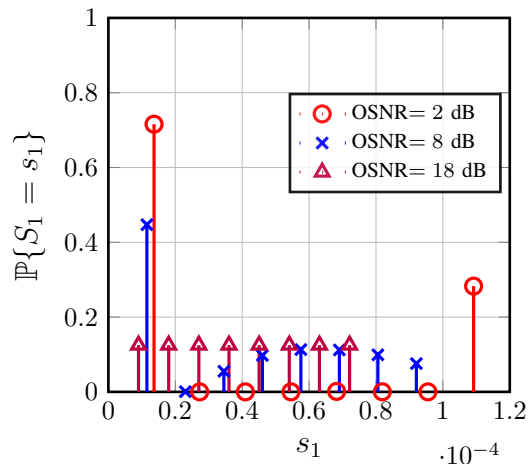


Figure 6: FER of NOMA for $M = 8$ and rate 1 bpcu.

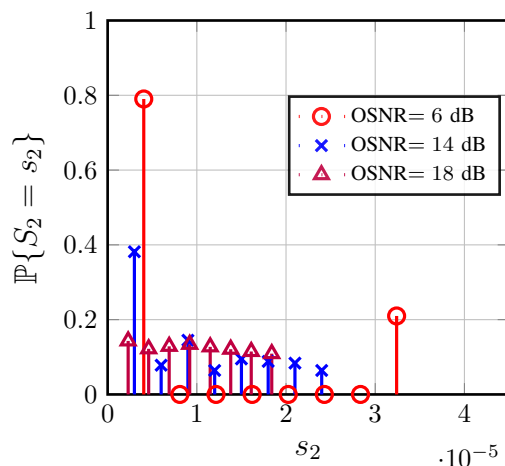
depicted in Fig. 5a, T_1 increases with the OSNR. R_{FEC}^* also rises with OSNR in order to maximize T_1 while satisfying the rate constraint, i.e., $T_1 \leq R_1^{\text{SDT}}$, where R_1^{SDT} is the AR of user 1. For example, R_{FEC}^* is $1/2$ at 1 dB and increases to a maximum value of $9/10$ at 12 dB. The optimum FEC rate for the uniform-distribution scheme is also chosen to achieve maximum T_1^u , but still ensures that it is below the capacity of the uniform signaling. As can be seen from Fig. 5a, at the OSNR region 2 – 4 dB, the proposed scheme operates within 0.05 bpcu and 0.25 bpcu from the capacity and its upper bound, respectively. Furthermore, at a rate of 0.75 bpcu, the proposed scheme outperforms uniform-distribution scheme by around 1.3 dB. However, at high OSNR, the gap between the TRs of the proposed and uniform-distribution schemes narrows for a fixed value of M . This is due to the fact that the conditional entropy of $X_j|\hat{Y}_j$ tends to zero at high OSNR, leaving only the entropy of X_j in the AR of user j . This entropy is maximized with a uniform distribution. Thus, it is recommended to switch to a higher M for higher OSNR.

Fig. 5b also shows the increase in R_{FEC}^* as a function of OSNR for user 2. The reason is similar as in the user 1. At the OSNR values of 6 dB and 15 dB, R_{FEC}^* is $1/3$ and $8/9$, respectively. Within the OSNR range of 7 – 9 dB, Fig. 5b demonstrates that the difference between the TR of proposed scheme and its capacity, as well as its upper bound, is about 0.1 bpcu and 0.3 bpcu, respectively. Additionally, at a rate of 0.75 bpcu, the proposed scheme outperforms the uniform-distribution scheme by approximately 2 dB. To achieve similar gains at higher OSNR, it is recommended to switch to a higher value of M . It is worth noting that the accuracy of the capacity upper bound varies for different users, as evident from Fig. 5. For example, the capacity upper bound provides a more accurate estimation for the user 2 than for the user 1.

To evaluate the performance of the proposed scheme, a comparison is made with the uniform-distribution, PCM, and GS schemes in terms of FER. Monte Carlo simulations are conducted, and the results are presented in Fig. 6. The TRs of users 1 and 2 are fixed at 1 bpcu, and the decoding utilizes the MAP values as computed in (18). The FER of user 1 is analyzed in Fig. 6a, and the minimum OSNRs required to achieve a TR of 1 bpcu can be determined from Fig. 5a. The capacity upper bound, \bar{C}_j , capacity of NOMA, C_j , AR of the proposed scheme, R_j^{SDT} , and capacity of NOMA with uniform signaling, C_j^u , provide reference points for these minimum OSNRs. Specifically, the respective values for user 1 are 2.5 dB, 4.6 dB, 5.3 dB, and 5.85 dB. Furthermore, the proposed scheme employs the optimal distribution, constellation spacing, and FEC rate, which are $\mathbf{p}_1^* = [0.5297, 0, 0, 0, 0.1709, 0, 0.0168, 0.2825]$, $\Delta_1^* = 1.0042 \times 10^{-5}$, and $R_{\text{FEC}}^* = 3/5$, respectively. For comparison, the PCM scheme utilizes $\mathbf{p}_1^{\text{pcm}} = [0.2949, 0.2949, 0, 0, 0, 0, 0.2051, 0.2051]$, $\Delta_1^{\text{pcm}} = 9.74 \times 10^{-6}$, and $R_{\text{FEC}}^{\text{pcm}} = 1/2$, while the GS scheme optimizes the spacing values to $\Delta_1^{\text{GS}} = [0.009, 4.566, 1.400, 4.798, 0.005, 0.002, 0.002, 0.001] \times 10^{-5}$. The uniform-distribution scheme uses $\mathbf{p}_1^u = (2P_{\tau_1})/(M+1)$, and $R_{\text{FEC}}^u = 1/3$ as its parameters. It is worth noting that the FER exhibits a phase transition



(a) User 1



(b) User 2

Figure 7: Optimized PMF for the constellation symbols when $M = 8$, for different instantaneous OSNRs.

phenomenon around the OSNR, corresponding to the TR. For example, at a FER of 10^{-3} , the proposed scheme outperforms the PCM, GS, and uniform-distribution schemes by approximately 0.3 dB, 0.4 dB, and 0.5 dB, respectively. In Fig. 6b, we examine the minimum OSNRs required for user 2 to achieve a TR of 1 bpcu, which are derived from Fig. 5b. The respective minimum OSNR values are 8 dB, 9.6 dB, 10.3 dB, and 17.7 dB for the capacity upper bound [23], capacity of NOMA, AR of the proposed scheme, and capacity of NOMA with uniform signalling. Furthermore, we determine the optimal parameters for user 2 in the proposed scheme, which are $\mathbf{p}_2^* = [0.7357, 0, 0, 0, 0, 0, 0.2643]$, $\Delta_2^* = 3.5 \times 10^{-6}$, and $R_{\text{FEC}}^* = 3/4$. Similarly, the PCM scheme employs $\mathbf{p}_2^{\text{pcm}} = [0.3659, 0.3659, 0, 0, 0, 0, 0.1341, 0.1341]$, $\Delta_2^{\text{pcm}} = 3.63 \times 10^{-6}$, and $R_{\text{FEC}}^{\text{pcm}} = 1/2$, while the GS scheme utilizes $\Delta_2^{\text{GS}} = [0, 0.1119, 0.0327, 0.1195, 0, 0, 0, 0]$ as the optimal spacing values for user 2. We can observe that, at a FER of 10^{-3} , the proposed scheme exhibits a gain of 0.6 dB, 1.3 dB, and 1.5 dB over the PCM, GS, and uniform-distribution schemes for user 2, respectively.

Fig. 7 provides a visualization of the optimized constellation

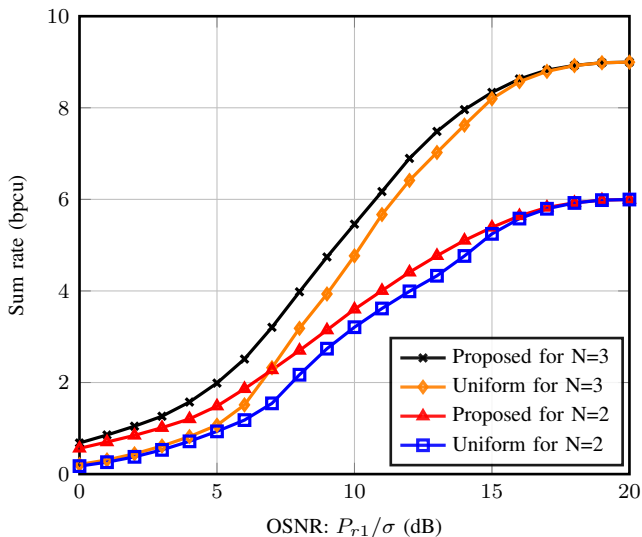


Figure 8: Maximum achievable sum rate (ASR) for $M = 8$.

symbols in the proposed scheme for each user at different OSNRs. At low OSNRs, as shown in Fig. 7a and Fig. 7b, symbols with the lowest amplitudes are assigned the highest probabilities. This assignment results in a larger inter-symbol spacing Δ_j^* , which satisfies the average optical power constraint and facilitates symbol detection in the presence of noise and interference. For example, the first and last constellation symbols of user 1 have probabilities of approximately $\mathbb{P}\{S_1 = \Delta_1^*\} = 0.7$ and $\mathbb{P}\{S_1 = 8\Delta_1^*\} = 0.3$ at the OSNR of 2 dB, while the probabilities of the remaining constellation symbols are negligible at the same OSNR. However, as the OSNRs increase, the distribution of constellation symbols becomes nearly uniform, causing the inter-symbol spacing to reduce. This behavior is evident from Fig. 5, where the gap between C_j and C_j^u diminishes at high OSNRs. Additionally, it is worth noting that the spacing between constellation points in Fig. 7b is smaller than in Fig. 7a due to the lower received power of user 2 relative to user 1.

In Fig. 8, we compare the maximum ASR of our proposed and the uniform-based schemes with $N = 2$ and $N = 3$ users for a broad range of OSNRs. The results clearly demonstrate that our proposed scheme consistently outperforms the uniform-based scheme for $N = 2$, showcasing the efficacy of our algorithm. With the introduction of an additional user, the performance gap in terms of the sum rate slightly widens due to increased number of users. For example, at OSNR = 6 dB, the performance gaps between the proposed and uniform-based schemes are around 0.8 bpcu and 1 bpcu for $N = 2$ and $N = 3$, respectively. To achieve similar gains at higher OSNR, it is recommended to switch to a higher value of M .

VII. CONCLUSION

In this paper, we proposed a novel adaptive coded PS-based NOMA scheme to enhance the SE in multiuser uplink VLC communication scenario. We derived the AR and TR of the proposed scheme. We introduced an alternate optimization algorithm to determine the capacity-approaching distribution

for each user for the given OSNR. This algorithm adaptively adjusts the channel coding rate and constellation spacing based on the OSNR. Our numerical results demonstrate that the proposed scheme achieves capacity of NOMA with fine granularity. Overall, the proposed scheme provides significant improvements in SE and FER over the PCM, GS and uniform-distribution schemes, making it a promising candidate for practical implementation in future VLC systems.

APPENDIX A CAPACITY OF NOMA

To determine capacity of NOMA, it is necessary to jointly optimize the distribution and spacing of the constellation symbols for every user. Consequently, there are N separate optimization problems that need to be solved sequentially.

First, after employing SIC technique, only the Gaussian-distributed noise remains in the received signal of the last decoded user, i.e., \hat{Y}_N . Hence, considering the power constraints described in Section II, we can determine the capacity of user N by solving the following optimization problem:

$$C_N = \underset{\Delta_N, \mathbf{p}_N}{\text{maximize}} R_N(\Delta_N, \mathbf{p}_N, \mathbf{a}_{\hat{y}_N}^*) \quad (42a)$$

$$\text{subject to } \mathbf{s}_N^T \mathbf{p}_N = P_{rN}, \quad (42b)$$

$$\frac{P_{rN}}{M} \leq \Delta_N \leq P_{rN}, \quad (42c)$$

$$\sum_{i=1}^M p_N^i = 1, \quad (42d)$$

$$p_N^i \geq 0, \quad \forall i \in \mathbb{M}, \quad (42e)$$

where $\mathbf{a}_{\hat{y}_N}^*$ is an empty vector because there is no interference from other users in the received signal of the last decoded user, i.e., \hat{y}_N , due to SIC.

Considering the prior decoded user received signal $\hat{Y}_{j < N}$, we observe the presence of interference from AWGN and multiuser interference from users $j+1$ to N . To ensure optimal distribution of the user $j < N$ signal, it is essential to account for this inter-user interference. For example, after obtaining \mathbf{p}_N^* and Δ_N^* from (42), the interference signal from user N in \hat{Y}_{N-1} follows the distribution given by \mathbf{p}_N^* and has spacing value Δ_N^* . Thus, the capacity for user $j < N$ can be subsequently obtained by solving the following optimization problem:

$$C_j = \underset{\Delta_j, \mathbf{p}_j}{\text{maximize}} R_j(\Delta_j, \mathbf{p}_j, \mathbf{a}_{\hat{y}_j}^*) \quad (43a)$$

$$\text{subject to } \mathbf{s}_j^T \mathbf{p}_j = P_{rj}, \quad (43b)$$

$$\frac{P_{rj}}{M} \leq \Delta_j \leq P_{rj}, \quad (43c)$$

$$\sum_{i=1}^M p_j^i = 1, \quad (43d)$$

$$p_j^i \geq 0, \quad \forall i \in \mathbb{M}, \quad (43e)$$

where $\mathbf{a}_{\hat{y}_j}^* \triangleq [\overline{\Delta}_{j+1}^*, \overline{\mathbf{p}}_{j+1}^*]$. The optimal PMFs and constellation values that maximize capacity for each user are determined using the inverse decoding order of the SIC, i.e., $N, N-1, \dots, 1$.

APPENDIX B
DERIVING THE KKT CONDITIONS

In the context of the convex optimization problem (35), the Lagrangian function can be expressed as

$$L = -T_j(\mathbf{p}_j) + \mu \left(\sum_{i=1}^M p_j^i - 1 \right) + \eta \left(R_{\text{FEC}} \sum_{i=1}^M \Delta i p_j^i - P_j \right) + \tau (T_j(\mathbf{p}_j) - \Phi(\mathbf{p}_j, \hat{\mathbf{p}}_j) + R_{\text{bf}}), \quad (44)$$

where $P_j \triangleq P_{rj} - (1 - R_{\text{FEC}}) \mathbf{s}_j^T \mathbf{p}_j^u$, and Lagrangian multipliers are denoted as μ , η and τ . To derive the KKT conditions, we differentiate the Lagrangian function L with respect to p_j^i and the Lagrangian multipliers μ and η , which are responsible for the equality constraints. Therefore, we have

$$\frac{dL}{dp_j^i} = R_{\text{FEC}} (\log(p_j^i) + 1) + \mu + \eta R_{\text{FEC}} \Delta i + \tau R_{\text{FEC}} W(i, \Delta_j, \hat{\mathbf{p}}_j, \mathbf{a}_{\hat{y}_j}^*) = 0, \quad (45)$$

$$\frac{dL}{d\mu} = \sum_{i=1}^M p_j^i - 1 = 0, \quad (46)$$

and

$$\frac{dL}{d\eta} = R_{\text{FEC}} \sum_{i=1}^M \Delta i p_j^i - P_j = 0. \quad (47)$$

The Lagrangian multiplier τ , which is responsible for non-equality constraint, results in two conditions.

Condition 1: $\tau = 0$

Equation (45) implies that

$$p_j^i = 2^{-1 - \frac{1}{R_{\text{FEC}}} \mu - \eta \Delta i}. \quad (48)$$

By replacing p_j^i in equation (46) with the expression from (48), μ becomes

$$\mu = -R_{\text{FEC}} + R_{\text{FEC}} \log \left(\sum_{i'=1}^M 2^{-\eta \Delta i'} \right). \quad (49)$$

Replacing μ in (48) with (49), p_j^i is

$$p_j^i = 2^{-\eta \Delta i - \log \left(\sum_{i'=1}^M 2^{-\eta \Delta i'} \right)} = \frac{2^{-\eta \Delta i}}{\sum_{i'=1}^M 2^{-\eta \Delta i'}}. \quad (50)$$

Due to the power constraint being an equality, the power constraint can be expressed as

$$\sum_{i'=1}^M (R_{\text{FEC}} \Delta i - P_j) 2^{-\eta \Delta i} = 0, \quad (51)$$

where (51) is derived by substituting p_j^i in (47) with (50).

Because $\tau = 0$, the rate constraint should be satisfied with strict inequality, i.e.,

$$T_j(\mathbf{p}_j) - \Phi(\mathbf{p}_j, \hat{\mathbf{p}}_j) + R_{\text{bf}} < 0 + R_{\text{FEC}} \sum_{i=1}^M p_j^i W(i, \Delta_j, \hat{\mathbf{p}}_j, \mathbf{a}_{\hat{y}_j}^*) + (R_{\text{FEC}} - 1) R_j(\Delta_j, \mathbf{p}_j^u, \mathbf{a}_{\hat{y}_j}^*) + R_{\text{bf}} < 0. \quad (52)$$

Substituting p_j^i in (52) with (50) implies that

$$\sum_{i=1}^M \left[R_{\text{FEC}} W(i, \Delta_j, \hat{\mathbf{p}}_j, \mathbf{a}_{\hat{y}_j}^*) - D \right] 2^{-\eta \Delta i} < 0, \quad (53)$$

where $D = (1 - R_{\text{FEC}}) R_j(\Delta_j, \mathbf{p}_j^u, \mathbf{a}_{\hat{y}_j}^*) - R_{\text{bf}}$.

Condition 2: $\tau > 0$

Equation (45) implies that

$$p_j^i = 2^{-1 - \frac{1}{R_{\text{FEC}}} \mu - \eta \Delta i - \tau W(i, \Delta_j, \hat{\mathbf{p}}_j, \mathbf{a}_{\hat{y}_j}^*)}. \quad (54)$$

Replacing p_j^i in (46) with (54), μ becomes

$$\mu = -R_{\text{FEC}} + R_{\text{FEC}} \log \left(\sum_{i'=1}^M 2^{-\eta \Delta i' - \tau W(i', \Delta_j, \hat{\mathbf{p}}_j, \mathbf{a}_{\hat{y}_j}^*)} \right). \quad (55)$$

Replacing μ in (54) with (55), p_j^i is

$$p_j^i = 2^{-\eta \Delta i - \tau W(i, \Delta_j, \hat{\mathbf{p}}_j, \mathbf{a}_{\hat{y}_j}^*) - \log \left(\sum_{i'=1}^M 2^{-\eta \Delta i' - \tau W(i', \Delta_j, \hat{\mathbf{p}}_j, \mathbf{a}_{\hat{y}_j}^*)} \right)} = \frac{2^{-\eta \Delta i - \tau W(i, \Delta_j, \hat{\mathbf{p}}_j, \mathbf{a}_{\hat{y}_j}^*)}}{\sum_{i'=1}^M 2^{-\eta \Delta i' - \tau W(i', \Delta_j, \hat{\mathbf{p}}_j, \mathbf{a}_{\hat{y}_j}^*)}}. \quad (56)$$

Considering the power constraint as an equality, the following equation should be satisfied

$$\sum_{i'=1}^M (R_{\text{FEC}} \Delta i - P_j) 2^{-\eta \Delta i - \tau W(i, \Delta_j, \hat{\mathbf{p}}_j, \mathbf{a}_{\hat{y}_j}^*)} = 0, \quad (57)$$

where (57) is derived by substituting p_j^i in (47) with (56).

When $\tau > 0$, the rate constraint is required to be satisfied with equality, i.e.,

$$R_{\text{FEC}} \sum_{i=1}^M p_j^i W(i, \Delta_j, \hat{\mathbf{p}}_j, \mathbf{a}_{\hat{y}_j}^*) + (R_{\text{FEC}} - 1) R_j(\Delta_j, \mathbf{p}_j^u, \mathbf{a}_{\hat{y}_j}^*) + R_{\text{bf}} = 0. \quad (58)$$

Substituting p_j^i in (58) with (56) implies

$$\sum_{i=1}^M \left[R_{\text{FEC}} W(i, \Delta_j, \hat{\mathbf{p}}_j, \mathbf{a}_{\hat{y}_j}^*) - D \right] \frac{2^{-\eta \Delta i}}{2^{\tau W(i, \Delta_j, \hat{\mathbf{p}}_j, \mathbf{a}_{\hat{y}_j}^*)}} = 0. \quad (59)$$

REFERENCES

- [1] M. A. Khalighi and M. Uysal, "Survey on free space optical communication: A communication theory perspective," *IEEE communications surveys & tutorials*, vol. 16, no. 4, pp. 2231–2258, Jun 2014.
- [2] H. Marshoud, S. Muhaidat, P. C. Sofotasios, S. Hussain, M. A. Imran, and B. S. Sharif, "Optical non-orthogonal multiple access for visible light communication," *IEEE Wireless Communications*, vol. 25, no. 2, pp. 82–88, Apr 2018.
- [3] H. Mathur and T. Deepa, "A survey on advanced multiple access techniques for 5G and beyond wireless communications," *Wireless Personal Communications*, vol. 118, pp. 1775–1792, Jan 2021.
- [4] G. Forney, R. Gallager, G. Lang, F. Longstaff, and S. Qureshi, "Efficient modulation for band-limited channels," *IEEE journal on selected areas in communications*, vol. 2, no. 5, pp. 632–647, Sep 1984.
- [5] Q. Wang, X. Pang, C. Wu, L. Xu, N. Zhao, and F. R. Yu, "Transmit power minimization for STAR-RIS aided FD-NOMA networks," *IEEE Transactions on Vehicular Technology*, Oct 2023.

- [6] A. M. Abdelhady, A. K. S. Salem, O. Amin, B. Shihada, and M.-S. Alouini, "Visible light communications via intelligent reflecting surfaces: Metasurfaces vs mirror arrays," *IEEE Open Journal of the Communications Society*, vol. 2, pp. 1–20, Dec 2020.
- [7] F. R. Kschischang and S. Pasupathy, "Optimal nonuniform signaling for Gaussian channels," *IEEE Transactions on Information Theory*, vol. 39, no. 3, pp. 913–929, May 1993.
- [8] J. Cho and P. J. Winzer, "Probabilistic constellation shaping for optical fiber communications," *Journal of Lightwave Technology*, vol. 37, no. 6, pp. 1590–1607, Feb 2019.
- [9] S. Javed, A. Elzanaty, O. Amin, B. Shihada, and M.-S. Alouini, "When probabilistic shaping realizes improper signaling for hardware distortion mitigation," *IEEE Transactions on Communications*, vol. 69, no. 8, pp. 5028–5042, Apr 2021.
- [10] G. Böcherer, F. Steiner, and P. Schulte, "Bandwidth efficient and rate-matched low-density parity-check coded modulation," *IEEE Transactions on Communications*, vol. 63, no. 12, pp. 4651–4665, Oct 2015.
- [11] A. Elzanaty and M.-S. Alouini, "Adaptive coded modulation for IM/DD free-space optical backhauling: A probabilistic shaping approach," *IEEE Transactions on Communications*, vol. 68, no. 10, pp. 6388–6402, Jul 2020.
- [12] A. Kafizov, A. Elzanaty, and M.-S. Alouini, "Probabilistic shaping based spatial modulation for spectral-efficient VLC," *IEEE Transactions on Wireless Communications*, Apr 2022.
- [13] S. Feng, T. Bai, and L. Hanzo, "Joint power allocation for the multi-user NOMA-downlink in a power-line-fed VLC network," *IEEE Transactions on Vehicular Technology*, vol. 68, no. 5, pp. 5185–5190, Mar 2019.
- [14] H. Sadat, M. Abaza, A. Mansour, and A. Alfalou, "A survey of NOMA for VLC systems: Research challenges and future trends," *Sensors*, vol. 22, no. 4, p. 1395, Feb 2022.
- [15] L. Yin, W. O. Popoola, X. Wu, and H. Haas, "Performance evaluation of non-orthogonal multiple access in visible light communication," *IEEE Transactions on Communications*, vol. 64, no. 12, pp. 5162–5175, Sept 2016.
- [16] B. Lin, Z. Ghassemlooy, X. Tang, Y. Li, and M. Zhang, "Experimental demonstration of optical MIMO NOMA-VLC with single carrier transmission," *Optics Communications*, vol. 402, pp. 52–55, Jul 2017.
- [17] Y. Xiao, P. D. Diamantoulakis, Z. Fang, Z. Ma, L. Hao, and G. K. Karagiannidis, "Hybrid lightwave/RF cooperative NOMA networks," *IEEE Transactions on Wireless Communications*, vol. 19, no. 2, pp. 1154–1166, Nov 2019.
- [18] M. Obeed, H. Dahrouj, A. M. Salhab, S. A. Zummo, and M.-S. Alouini, "User pairing, link selection, and power allocation for cooperative NOMA hybrid VLC/RF systems," *IEEE Transactions on Wireless Communications*, vol. 20, no. 3, pp. 1785–1800, Mar 2020.
- [19] R. Xu, Z. Wang, J. Yu, and S. Han, "Investigation on probabilistic shaping for symbol-level uplink non-orthogonal multiple access visible light communication systems," in *Proc. of the 20th International Conference on Communication Technology (ICCT), 28-31 October 2020, Nanning, China*. IEEE, Dec 2020, pp. 605–610.
- [20] P. Schulte and G. Böcherer, "Constant composition distribution matching," *IEEE Transactions on Information Theory*, vol. 62, no. 1, pp. 430–434, Nov 2015.
- [21] K. Lange, D. R. Hunter, and I. Yang, "Optimization transfer using surrogate objective functions," *Journal of computational and graphical statistics*, vol. 9, no. 1, pp. 1–20, Feb 2000.
- [22] P. O. Vontobel, A. Kavcic, D. M. Arnold, and H.-A. Loeliger, "A generalization of the Blahut-Arimoto algorithm to finite-state channels," *IEEE Transactions on Information Theory*, vol. 54, no. 5, pp. 1887–1918, Apr 2008.
- [23] A. Chaaban, O. M. S. Al-Ebraheemy, T. Y. Al-Naffouri, and M.-S. Alouini, "Capacity bounds for the Gaussian IM-DD optical multiple-access channel," *IEEE Transactions on Wireless Communications*, vol. 16, no. 5, pp. 3328–3340, Mar 2017.
- [24] L. Yin, X. Wu, and H. Haas, "On the performance of non-orthogonal multiple access in visible light communication," in *Proc. of the 26th Annual International Symposium on Personal, Indoor, and Mobile Radio Communications (PIMRC), 30 Aug - 2 Sept 2015, Hong Kong, China*. IEEE, Dec 2015, pp. 1354–1359.
- [25] T. Fath and H. Haas, "Performance comparison of MIMO techniques for optical wireless communications in indoor environments," *IEEE Transactions on Communications*, vol. 61, no. 2, pp. 733–742, Dec 2012.
- [26] R. Mesleh, H. Elgala, and H. Haas, "Optical spatial modulation," *IEEE/OSA Journal of Optical Communications and Networking*, vol. 3, no. 3, pp. 234–244, Mar 2011.
- [27] A. A. Farid and S. Hranilovic, "Channel capacity and non-uniform signalling for free-space optical intensity channels," *IEEE Journal on Selected Areas in Communications*, vol. 27, no. 9, pp. 1553–1563, Dec 2009.
- [28] N. Zhang, J. Wang, G. Kang, and Y. Liu, "Uplink nonorthogonal multiple access in 5G systems," *IEEE Communications Letters*, vol. 20, no. 3, pp. 458–461, Jan 2016.
- [29] "White paper on the use of DVB-S2X for DTH applications, DSNG & professional services, broadband interactive services and VL-SNR applications," Digital Video Broadcasting, Tech. Rep., Mar 2015.
- [30] E. Biglieri, *Coding for wireless channels*. Springer Science & Business Media, New York, 2005.
- [31] G. Böcherer, P. Schulte, and F. Steiner, "Probabilistic shaping and forward error correction for fiber-optic communication systems," *Journal of Lightwave Technology*, vol. 37, no. 2, pp. 230–244, Jan 2019.
- [32] F. A. Potra and S. J. Wright, "Interior-point methods," *Journal of Computational and Applied Mathematics*, vol. 124, no. 1-2, pp. 281–302, Nov 2000.
- [33] Z. He, T. Bo, and H. Kim, "Probabilistically shaped coded modulation for IM/DD system," *Optics express*, vol. 27, no. 9, pp. 12 126–12 136, Apr 2019.



Amanat Kafizov received his B.Sc. and M.Sc. degrees in Electrical and Computer Engineering from Nazarbayev University, Kazakhstan, in 2019 and from King Abdullah University of Science and Technology (KAUST), Saudi Arabia, in 2021, respectively. Currently, he is a Ph.D. student at KAUST. His academic journey has been enriched by diverse experiences, including a summer research internship at the University at Buffalo, New York, USA, in 2018, where he developed OFDM system for Terahertz communication. Later, from 2023 to

2024, he worked as a research engineer at CERN, Geneva, Switzerland, focusing on the high granularity calorimeter (HGCAL). His research interests include visible light communication, reconfigurable intelligent surfaces, coded modulation, uneven distribution, and machine learning.



Ahmed Elzanaty (S12-M18-SM21) received the Ph.D. degree (excellent cum laude) in electronics, telecommunications, and information technology from the University of Bologna, Italy, in 2018, where he was a Research Fellow from 2017 to 2019. He was a Postdoctoral Fellow with the King Abdullah University of Science and Technology, Saudi Arabia. He is currently a Lecturer (Assistant Professor) at the Institute for Communication Systems, University of Surrey, United Kingdom. He has participated in several national and European projects, such as GRETA and EuroCPS. His research interests include the design and performance analysis of wireless communications and localization systems, cellular network design with EMF constraints, coded modulation, wireless localization, compressive sensing, and distributed training of neural networks.

as GRETA and EuroCPS. His research interests include the design and performance analysis of wireless communications and localization systems, cellular network design with EMF constraints, coded modulation, wireless localization, compressive sensing, and distributed training of neural networks.



Mohamed-Slim Alouini (S94-M98-SM03-F09) was born in Tunis, Tunisia. He received the Ph.D. degree in Electrical Engineering from the California Institute of Technology (Caltech) in 1998. He served as a faculty member at the University of Minnesota then in the Texas A&M University at Qatar before joining in 2009 the King Abdullah University of Science and Technology (KAUST) where he is now the Al-Khawarizmi Distinguished Professor of Electrical and Computer Engineering. Prof. Alouini is a Fellow of the IEEE and OPTICA (Formerly the

Optical Society of America (OSA)). He is currently particularly interested in addressing the technical challenges associated with the uneven distribution, access to, and use of information and communication technologies in rural, low-income, disaster, and/or hard-to-reach areas.